NDT and E International 101 (2019) 53–61

Contents lists available at ScienceDirect

NDT and E International

journal homepage: www.elsevier.com/locate/ndteint

Detection and assessment of pitting corrosion in rebars using scattering of ultrasonic guided waves

Rajeshwara Chary Sriramadasu[a,b,c], Sauvik Banerjee[b,*], Ye Lu[c]

[a] IITB-Monash Research Academy, Indian Institute of Technology Bombay, Powai, Mumbai, 400076, India
[b] Department of Civil Engineering, Indian Institute of Technology Bombay, Powai, Mumbai, 400076, India
[c] Department of Civil Engineering, Monash University, Clayton, VIC, 3800, Australia

ARTICLE INFO

Keywords:
Pitting corrosion
Non-destructive evaluation
Damage index
Scatter coefficient
Reinforcement bars

ABSTRACT

The present study aims at developing a robust non-destructive evaluation technique by using the scattering of ultrasonic guided waves for early detection and assessment of localised damage in bare rebars in the form of corrosion pits. The guided wave interaction with the pitting corrosion is numerically simulated by using finite element analysis, and the results are validated with experiments. The received signal contains several wave packets, which could be identified as various scattered modes that are generated from the edges of the corroded region. It is found that when the damage is placed at the centre of the rebar, several scattered wave modes superimpose to form two distinct wave packets in the received signal. A damage index is proposed by using these two distinct wave packets. It is shown that the proposed damage index method can be used successfully to monitor the axial extent and intensity of pitting corrosion in rebars. However, for the pitting corrosion that is situated at an arbitrary position, a different methodology, which utilises the differential time of arrival of various scattered wave modes, is proposed to identify the location of the pitting corrosion. Finally, a non-dimensional parameter, namely the scatter coefficient, is defined to analyse the energy contributions of various scatter modes. It is found that this scatter coefficient gradually increases with the mass loss and that the increment is pronounced when the corrosion pit is closer to the receiver location. The findings of the study can be used to identify the pitting corrosion in bare rebars.

1. Introduction

Reinforcement bars are widely used in civil structures to enhance the tensile strength of concrete. Corrosion of reinforcement bars has been a major cause of concern for researchers as it can result in catastrophic failure of infrastructure. In reinforced concrete (RC) structures, concrete provides the alkaline environment and thus forms a passive layer around the rebars. But, ingress of excessive acidic agents such as chlorine deteriorate this passive layer. The corrosion product that is generated due to this process gets debonded from the intact rebar and results in a reduction of diameter. This reduction in the effective diameter of the rebar leads to a lower moment of resistance, leading to failure of structural components [1].

Guided waves are being increasingly used in the aerospace industry for their utility in the identifying of cracks, debonding and delamination in aluminium plates and composite structures [2–5]. Studies have indicated that they can travel over a long distance with low attenuation. Thus, guided wave based techniques can be used scan damages in a large area with fewer measurements compared to conventional chemical methods like half-cell potential measurements, concrete carbonation test, etc. and mechanical methods like ultrasonic pulse velocity test, rebound hammer test, etc. [6–8]. By utilising the dispersion properties of guided waves, studies were successful in identifying and generating specific wave modes which have dominant variation in the wave characteristics due to a specific type of damage [9]. This success inspired various researchers to deploy guided waves in the identifying of defects in reinforced cement concrete (RCC) structures in the recent years [10–12].

It is widely stated in the literature that the corrosion process in a reinforced concrete (RC) leads to a reduction in the diameter as well as in the debonding at the concrete-steel interface. Various researchers have studied the discrete effect of each of these two features of corrosion. In recent studies, it has been expressed that the diameter reduction and debonding have a complementary effect on the wave characteristics [13]. The co-occurrence of these two types of damage is studied, and through numerical simulations, it has been shown that a concealed

* Corresponding author.
E-mail addresses: rcsriramadasu@gmail.com (R.C. Sriramadasu), sauvik@civil.iitb.ac.in (S. Banerjee).

https://doi.org/10.1016/j.ndteint.2018.10.005
Received 26 April 2018; Received in revised form 12 September 2018; Accepted 9 October 2018
Available online 09 October 2018
0963-8695/

state of damage that is known as the zero effect state can occur in a corroded rebar RC structure [14]. It has become imperative to develop damage identification algorithms to detect such concealed damage in rebars.

Corrosion in rebars can be classified into uniform corrosion and pitting corrosion. Carbonation of concrete causes microcell corrosion in which a numerous number of small corrosion cells are formed over a large length of rebar. This effect causes the cross section of rebar to reduce in a large length of rebar. This type of corrosion is termed as uniform corrosion. This type of corrosion is often slow and can be detected and controlled easily. Recently, embeddable piezoelectric patches were successfully tested to detect and quantify uniform corrosion in RC structures [15]. Low chloride concentration often results in the formation of macro-cell corrosion in rebars. In this type of corrosion, a small portion of the rebar with high negative potential acts as anode and rest of the rebar acts as a cathode. Corrosion of the rebar occurs at the anodic site and cross section of this portion gets reduced due to the formation of rust. This type of corrosion is termed as localised corrosion or pitting type of corrosion [16]. The pitting type of corrosion can occur and propagate at a faster rate. It is recognised to be more dangerous because the cross section of the rebar is reduced to a point at which the load-carrying capacity of the rebar is completely diminished and a catastrophic failure of the structure is enforced [1,17].

ToF obtained from various wavelet transforms has been used to detect uniform corrosion. The differential ToF of L (0, 1) mode from an undamaged rebar and a corroded rebar has been used to identify the corrosion state in various uniformly corroded rebar samples. It is reported that the differential ToF increases with the intensity of the corrosion in the rebar [18]. However, the dominant change in the ToF and the amplitude of wave modes, which is observed due to uniform corrosion, could not be witnessed in the case of pitting corrosion. Hence, the methods that are developed for uniform corrosion do not hold good for pitting corrosion. The pitting corrosion in pipelines is widely studied in the literature by correlating the reflection characteristics of guided waves with the damage sizes [19–21]. A. Demma et al. [22] have investigated the dependence of reflection coefficient on circumferential extent and depth of defect in pipelines by using torsional T (0,1) mode and have proposed reflection maps to quantify unknown defects in pipelines.

Pitting corrosion in rebars is detected and assessed by using ultrasonic guided waves in this study. The longitudinal guided wave mode, L (0, 1), is excited by using contact-type transducers that are attached to the ends of the rebar. The variation in amplitude measurements due to bonding between the transducer and the structure is eliminated by normalising the signal with respect to the peak amplitude of the L (0, 1) mode. The response of the rebar with pitting corrosion is analysed and various wave modes in the signal are identified. The scattered modes that are generated due to the presence of damage can imitate the damage intensity and boundaries. The characteristics of the scattered waves are predicted by testing rebars at various corrosion levels.

In the recent years, damage index methods have become popular because of their capability to indicate the presence of damage. The uncertainty in damage identification is well accounted by using damage index algorithms because they give the statistical probability of damage occurrence at any location. Damage indices were proposed by researchers by using signal amplitude, FFT energy, wavelet coefficients and principal components [10], [23,24]. In this study, a damage index that is based on the Hilbert coefficients is proposed for the damages that are located near the centre of the rebar. The efficacy of this method is evaluated for accurate identification of corrosion in bare rebars. However, the corrosion that is located at an arbitrary location is identified by retracing the damage boundaries by using the differential time of arrival of various scattered wave modes. A non-dimensional parameter, namely the scatter coefficient is defined to analyse various levels of corrosion that are located at the centre as well as away from the centre.

2. Wave propagation in reinforcement bar with damage

The propagation of energy in a body with the aid of the movement of particles in the body can be described as wave propagation. Wave propagation is extensively used in the study of the mechanical behaviour of a material. The changes in mechanical properties affect the propagation characteristics of various wave modes, and this property is extensively used for damage identification. In this section, the theory of guided waves in a cylindrical medium is presented, and the various scattering modes that are generated due to corrosion damage are discussed.

The wave propagation in a cylindrical waveguide is governed by equation (1)

$$(\lambda + \mu)\nabla\nabla\cdot\mathbf{U} + \mu\nabla^2\mathbf{U} + \rho f = \rho\ddot{\mathbf{U}} \tag{1}$$

where **U** is the displacement vector, f is the body force vector, ρ is the density, and λ and μ are Lamé constants. The solution that was suggested by Gazis for the governing equation above is considered to hold good for longitudinal waves [25]. An alternative solution that was proposed by Sun et al. can be used to estimate longitudinal as well as torsional modes [26]. The displacement vector, **U**, can be expressed as in equation (2) by using Helmholtz decomposition as the sum of the gradient of scalar potential, Φ, and curl of zero divergence vector, H.

$$U = \nabla\varphi + \nabla \times H \text{ and } \nabla\bullet H = 0 \tag{2}$$

The general solution that was presented by Sun et al. is given by equation (3)

$$\begin{aligned} &\phi = f(r)e^{im\theta}e^{i(kz-\omega t)} \quad H_r = h_r(r)e^{im\theta}e^{i(kz-\omega t)} \\ &H_\theta = h_\theta(r)e^{im\theta}e^{i(kz-\omega t)} \quad H_Z = h_z(r)e^{im\theta}e^{i(kz-\omega t)} \end{aligned} \tag{3}$$

Three traction-free boundary conditions on the outer surface and the gauge invariance condition for an infinitely long reinforcement bar lead to an eigenvalue problem, [C][A] = 0, in which **C** is a 4×4 matrix. The detailed solution of the above equations can be found in Ref. [6]. Theoretical dispersion curves can be plotted by using the eigenvalues of equation (3). The presence of damage and changes in the interface conditions render a complicated form to the set of analytical equations that is mentioned above. Hence, numerical solutions are employed to solve such problems.

The existence of corrosion in reinforcement leads to contamination of the received signal due to scattering at the damage edges. The change in the geometric properties of the reinforcement necessitates a change in the group velocity in the damaged area. Hence, a change in the ToF can be observed in that area. However, this change in the ToF cannot result in an appreciable change in the ToF of the initially transmitted signal of the entire structure.

Depending upon the location and relative size of damage, with respect to the reinforcement bar, an infinite number of modes is possible. The prevalence of any particular mode depends on the incident wave energy and reflection coefficients. A few basic scattered modes that occur due to the front and rear edges of damage are shown in Fig. 1. A part of the initial signal is unaffected by the damage and arrives at the sensor at a time, T. The times of flight for various portions of the rebar are indicated by t1, t2 and t3. Arrival times for various damage-scattered modes are listed in Table 1. These modes can be identified in the numerical and experimental signal with their arrival times.

The received signal takes a simplified form when the damage is located equidistant from the actuator and sensor (that is, t1 = t3). In such a case, the scattered wave modes 3 and 5 arrive at the same time. Simillarly, two sets of scattered wave modes (6, 7) and (9, 10) also arrive at the same time. Thus, in the received signal, these two sets of scattered wave packets form two distinct peaks, which were observed in the numerical simulations and experiments. In this study, the effect of rebar corrosion on the characterstics of various scattered wave packets is analysed.

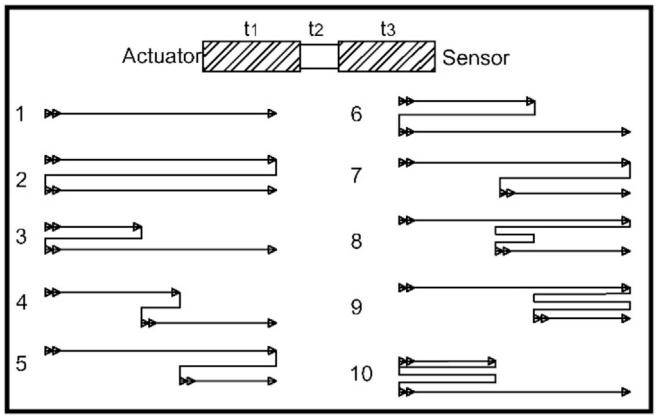

Fig. 1. Scattering pattern in damaged rebar.

Table 1
Scattered wave modes and their arrival times at the sensor.

Mode No.	Time of arrival at sensor	Mode No.	Time of arrival at sensor
1	T	6	T + 2*t1 + 2*t2
2	3T	7	T + 2*t2 + 2*t3
3	T + 2*t1	8	T + 4*t2 + 2*t3
4	T + 2*t2	9	T + 4*t3
5	T + 2*t3	10	T + 4*t1

3. Numerical modelling and experimental validation

A numerical model of rebar with a simply supported boundary condition is developed in Abacus/CAE 6.14, a finite element analysis (FEA) software. The length and diameter of the rebars are 600 mm and 20 mm, respectively. Material properties of the rebar are listed in Table 2. A mesh size of 2 mm and time increment of 1×10^{-7} s are used to satisfy the Courant–Friedrich–Levy condition [27].

The effect of ribs on rebar has been studied by a few researchers and the key finding of their research is that the presence of ribs does not affect the signal when the ratio of the wavelength to the dimension of the ribs is high [28], [29–31]. The typical rib dimension for a 20 mm rebar is in the range of 1.25 mm–1.35 mm. The frequency of the testing that is used in this study is 100 kHz. The wavelength-to-rib dimension is estimated to be greater than 2, which indicates that the ribs have a limited effect on wave characteristics. Therefore, a simplified solid rebar model is used instead of ribbed rebar for simulation. A five-cycle Hanning pulse at 100 kHz is applied at one end of the rebar to generate longitudinal waves. A rebar without damage is used as a baseline. The baseline signal shows a clear transmission signature at a time, 'T', and boundary echo after time, '3T'. Corrosion is simulated in rebar by reducing the diameter of the selected portion while keeping all the other modelling parameters unchanged.

Rebar samples, such as those that are shown in Fig. 2(a) with various corrosion intensities, axial extents, and locations were used in experiments to verify the simulation results. The corrosion in the rebar samples is achieved by scrapping off the material from the surface of these samples. A schematic diagram of a pristine rebar and a rebar with corrosion damage that is located at the centre, with an axial extent of 100 mm, is shown in Fig. 2(b). The ends of these samples were flattened and contact transducers of diameter 12.5 mm (supplied by Olympus)

Table 2
Material properties of rebar.

Material	Density (kg/m^3)	Poisson ratio	Young's Modulus (GPa)
Steel	7850	0.30	200

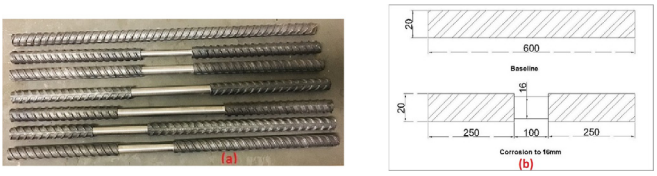

Fig. 2. (a) Rebar samples used in the experiment and (b) a typical reinforcement bar used as a baseline, and a reinforcement bar with corrosion.

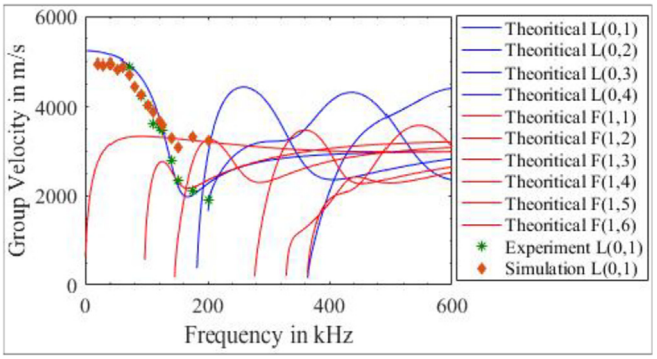

Fig. 3. Group velocity dispersion curves for a 20 mm rebar.

were attached in order to generate longitudinal waves. A Tektronix arbitrary function generator, AFG 3102, was used to generate input signal. The response signal is collected at the receiver end by a digital oscilloscope, DPO1034B, at a sampling frequency of 10 MHz. Averaging of the response signal over 512 cycles is achieved by using an inbuilt function in the oscilloscope.

Dispersion curves for a rebar with a diameter of 20 mm are plotted by using DISPERSE software [32]. The group velocity is obtained from numerical results for each of the frequencies of excitation by dividing the length of the rebar with ToF, which is calculated by the differential time from the peak input to the peak output signals. These dispersion curves, as shown in Fig. 3, were verified by using group velocities that were obtained through experiments on the undamaged rebar. From the dispersion curves, it is observed that only one longitudinal mode is possible for axisymmetric geometry in the frequency range of 0–150 kHz. A five-cycle Hanning pulse with 100 kHz central frequency is selected for signal actuation as longitudinal mode, L (0, 1), can be excited with less dispersion. The responses of an undamaged specimen that was collected using simulation and experiments are compared in Fig. 4(a). The direct transmitted signal and the boundary reflected signal could be recognised from the energy envelopes of the signals by using the Hilbert coefficients [33], as shown in Fig. 4(b). The input frequency of 100 kHz results in a dominant L (0, 1) mode, which has an arrival time of 129.5 μs in the simulation. Additionally, it is comparable to the arrival time (125.2 μs) of the direct transmitted signal that is observed in the experiments.

Fig. 5 shows a typical comparison of FEA and experimental signals for a 100 mm-wide corrosion of rebar with a diameter reduction to 16 mm diameter from 20 mm diameter. The effective diameter of the rebar is reduced in the numerical simulation by deleting the elements in the specific portion of the rebar. The response of rebars with corrosion damage shows the wave packets that were generated due to scattering from damage edges, which were similar to the simulation results. This damage-scattered signal can be utilised to study the effect of a change in the intensity, axial extent and location of pitting corrosion, which will be addressed in section 4. In the rebar in which the corrosion is located at the centre, two distinct wave packets can be observed in the signal, as will be explained in section 4.1 and section 4.2. These wave packets are analysed in order to develop a damage index method. In the rebar in which the damage located away from the centre, more than

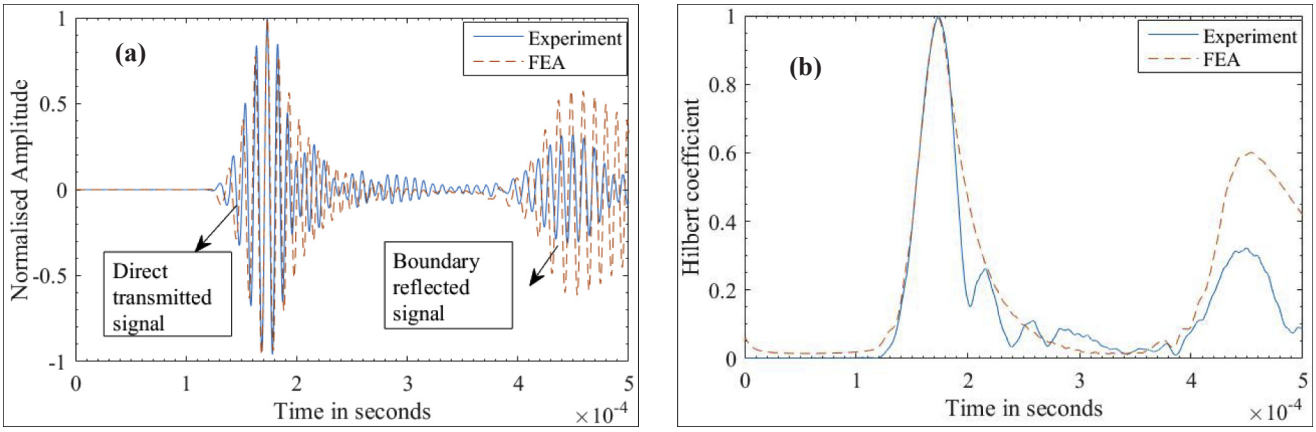

Fig. 4. (a) Comparison of baseline signal from experiment and FEA and, (b) comparison of energy envelope of baseline signal from experiment and FEA.

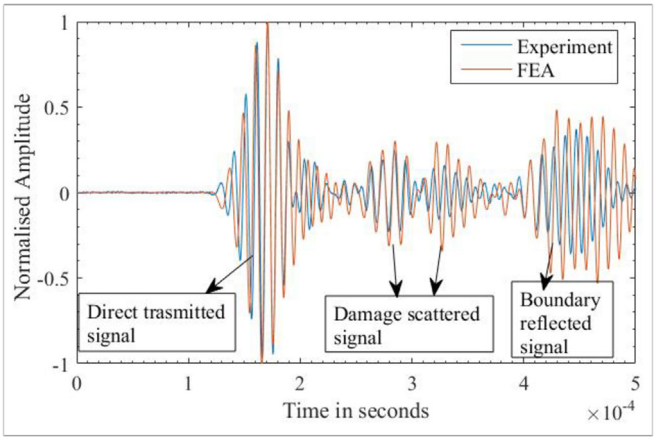

Fig. 5. Comparison of FEA and experiment signal of rebar with 100 mm-wide corrosion located at the centre.

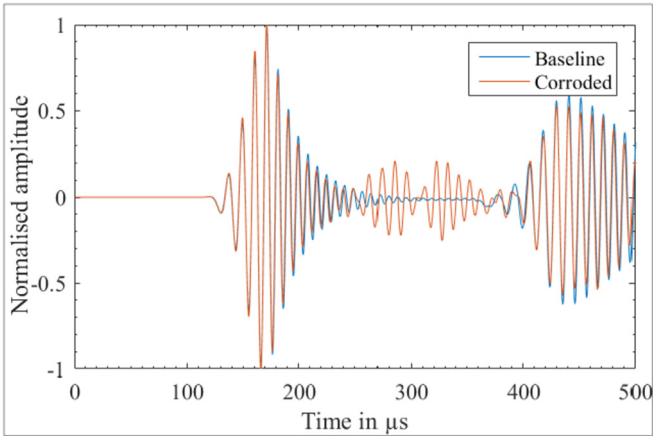

Fig. 6. Comparison of the signal from a corroded rebar with baseline signal by using FEA.

two packets are observed, as will be explained in section 4.3, four of which are significant and are used to identify the damage.

4. Results and discussion

From numerical studies and experiments, it is observed that the presence of damage results in scattering of wave energy. The wave packets that are generated due to scattering are examined in this study to develop a method to ascertain the progress of the damage. Three types of variations in corrosion are examined. First, the intensity of corrosion is varied for a fixed axial extent of corrosion at the centre by reducing the diameter of rebar in the corroded region. The radial profile of the pitting corrosion is maintained as circular for computational simplicity. Second, the axial extent of corrosion is varied for a fixed reduction in diameter at the centre. Third, the location of corrosion is varied while maintaining the intensity and axial extent of corrosion as constant.

4.1. Assessment of corrosion in a rebar with varying corrosion intensity

In order to examine the effect of corrosion, rebars with various intensities of corrosion are modelled and the results are compared with the baseline signal. Fig. 6 shows the comparison between signals with and without a 100 mm-wide corrosion that is located at the centre with a diameter reduction to 16 mm. Fig. 7 shows the energy envelope that is plotted using a Hilbert transform [33] of the signals. Two distinct peaks can be observed in the signal of the corroded sample, and this effect can be attributed to the scattering from the edges of the damage.

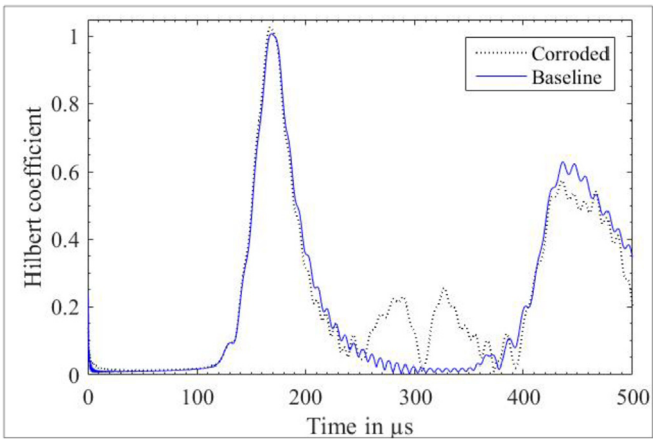

Fig. 7. Comparison of energy envelopes of the signal from corroded rebar with baseline signal by using FEA.

It is further observed that an increase in corrosion of the rebar results in an increase in the amplitude of scattered wave packets. The differential time of arrival of the two wave packets has a direct correlation with the boundaries of the damage. A damage index is therefore developed by using the reflection pattern that occurs due to the pitting type of the corrosion that is located at the centre of the rebar. In this method, the rebar is discretised into n elements with n + 1 nodes, as shown in Fig. 8. The boundary of the damage is assumed to exist at each of the nodes, and the damage index is calculated. The path that is

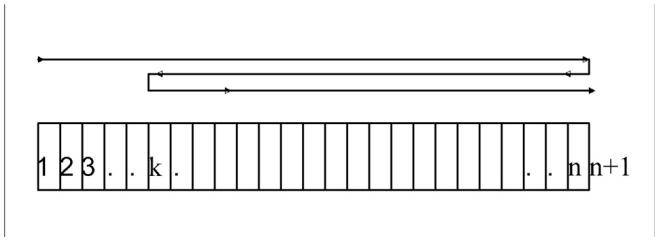

Fig. 8. Discretisation in a typical rebar for damage index calculation, and path of the signal in case of damage at the node, k.

followed by the scattered wave for a damage boundary that is located at the kth node is shown in Fig. 8. Typically, if there is no damage the value of the damage index will be zero. The damage index at each node is defined by the following equation:

$$DI(x) = \sqrt{\int_{t1}^{t2} (S - B)^2 dt} \tag{4}$$

where $t1 = (L + 2*x)/V$

$t2 = t1 + \Delta$

V is the velocity of the specific mode.

L is the length of rebar.

x is the distance of a node from the sensor.

Δ is the bandwidth of the input pulse (50 μs for 100 kHz).

S is the signal from the specimen with damage.

In the current case, the length of the damage is maintained at 100 mm, and the diameter of the corroded portion is reduced. The damage index of various corroded rebar samples, which was calculated by using FEA signal, is shown in Fig. 9. It can be observed from the figure that the value of the damage index increases with an increase in the level of corrosion. The front and rear edges of the damage have a high damage index as there is change in the cross section. This high damage index can be used to monitor the progress of the corrosion in the rebar. In detail, the peak in the damage index plot indicates the location of the damage edge, while the area under the curve for each case of damage can be used in order to estimate the intensity of corrosion. An estimate of the axial length of corrosion, which is obtained from the peak-to-peak distance in the damage index plot, is listed in Table 3, showing excellent agreement with actual length of corrosion.

The results of the simulation are verified with experimental results in a few cases. A comparison of the signal of the corroded rebars with the baseline that was obtained from experiments is shown in Fig. 10. In line with the simulation results, the signal from a corroded rebar has scattered wave packets, which form two distinct wave packets. The

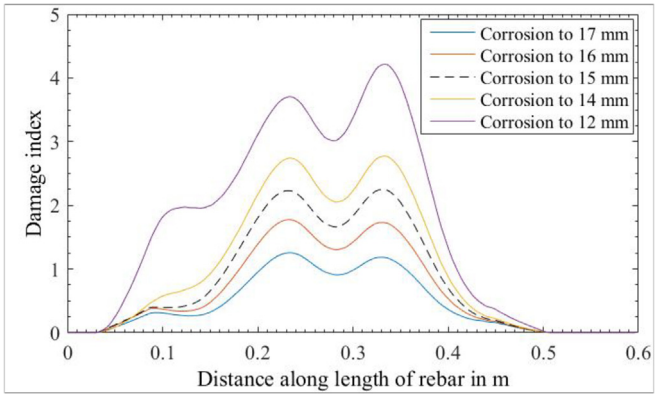

Fig. 9. Damage index of steel bars with various intensities of corrosion located at the centre.

Table 3
Estimation of damage length using damage index plot for a 100 mm-wide corrosion damage in rebar (FEA).

Reduced diameter (mm)	First peak (mm)	Second peak (mm)	Damage size (mm)	Error in length estimation (%)
17	234	330	96	4%
16	234	330	96	4%
15	231	333	102	2%
14	234	333	99	1%
12	231	333	102	2%

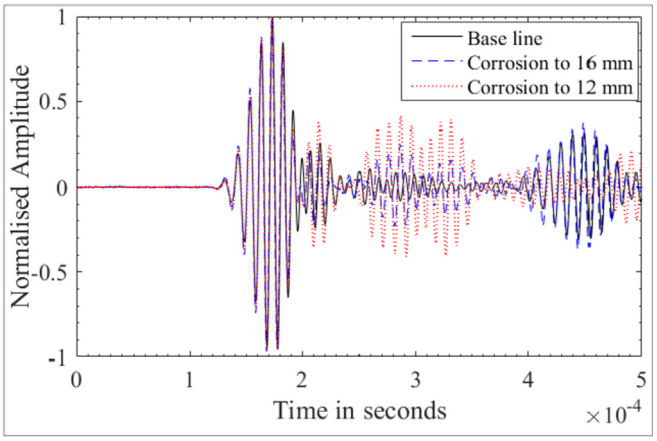

Fig. 10. Comparison of the signal from rebars with various intensities of corrosion by using experiments.

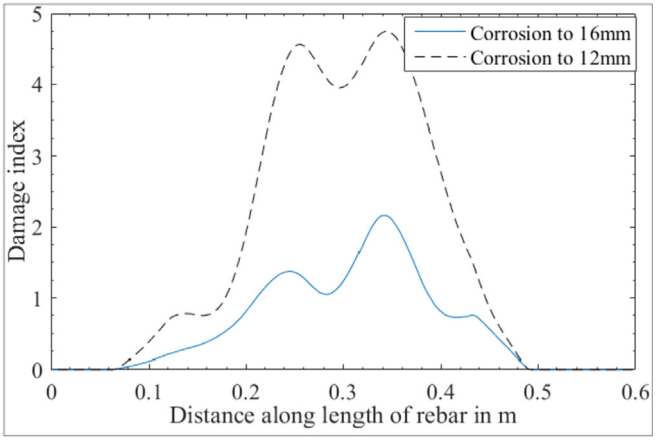

Fig. 11. Damage index plots for rebars with various levels of corrosion by using experiments.

damage index is calculated by using the experimental signals and it is plotted against each of the discretised nodes. It can also be observed that the increase in the corrosion intensity results in an increase in the damage index, as shown in Fig. 11. Hence, the progression of the corrosion due to the change in the intensity can be monitored by using the proposed method. The estimation of the length of the corroded portion by using the damage index is presented in Table 4 for a few experimental specimens, showing good agreement with actual length of corrosion as well.

4.2. Assessment of corrosion in a rebar with varying axial extents of corrosion

The corrosion in a rebar can also progress due to an increase in the

Table 4
Estimation of corrosion length from damage index plots by using experimental signals.

Corroded rebar diameter (mm)	First peak (mm)	Second Peak (mm)	Damage size (mm)	Error in length estimation (%)
16	246	342	96	4%
12	255	345	90	10%

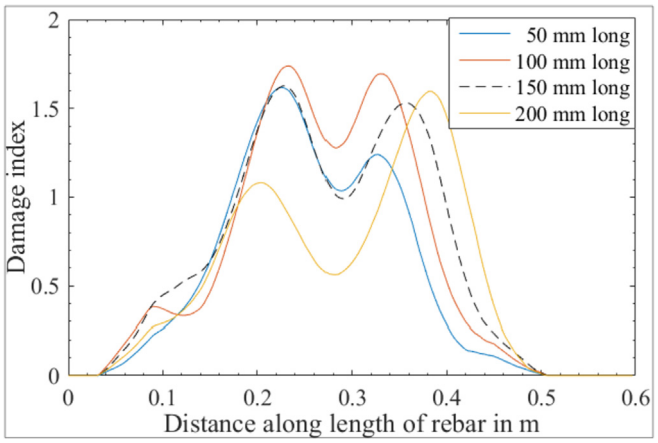

Fig. 12. Damage index plot for various lengths of damage located at the centre by using FEA.

Table 5
Estimation of corrosion length using damage index plot for damage that is equidistant from transducers.

Corrosion length (mm)	Damage size estimated from simulation (mm)	Error (%) (Simulation)	Damage size estimated from experiment (mm)	Error (%) (Experiment)
50	102	100%	–	–
100	99	4%	96	4%
150	129	14%	132	12%
200	178	11%	192	4%

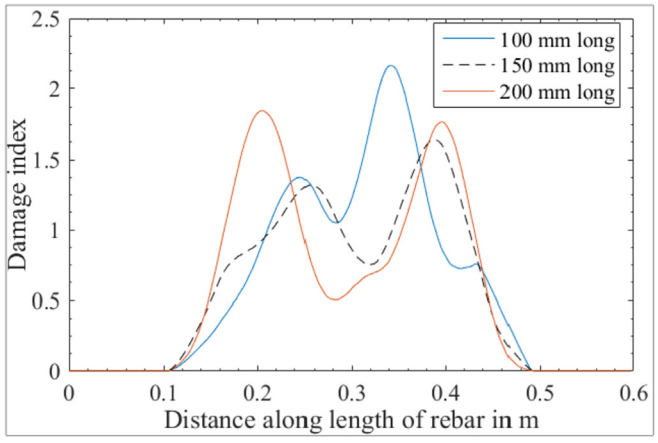

Fig. 13. Damage index plot for various lengths of damage located at the centre by using experiments.

length of the corroded portion. Hence, various rebars with the varying axial extents of corrosion for the same reduction in diameter were studied by using FEA and experiments. It is observed that the differential time of arrival of the scattered wave packets increases with the increase in the length of the corroded portion. The damage index that is similar as defined in section 4.1 can be used to monitor this category of pitting corrosion progression in the rebar. Damage index that is calculated by using FEA signals in a few cases of corrosion with different lengths of corrosion is shown in Fig. 12. In the figure, the damage index that is obtained for corrosion cases of the axial extents of 100 mm, 150 mm and 200 mm clearly shows the edges of corrosion damage. Hence, the pitting corrosion can be monitored when its progress is along the axial direction. The lengths of the corroded portion that is calculated for the FEA signals by using the damage index plots are listed in Table 5. The simulation results are verified by using damage index plots of the signal from experiments, as shown in Fig. 13. The length of the damage, which was estimated from experiments, is in agreement with simulation results that are presented in Table 5.

On the other hand, in the case of the corrosion with an axial extent of less than a cut-off length, it is observed that damage could not be quantified by using the damage index that is defined in this study. This is because the distinct peaks in received signal from damage edges could only be observed when the damage is larger than the cut-off length. Numerical models with various lengths of damage are analysed, and the cut-off length for the current case is 70 mm. As can be observed in the pitting corrosion that has an axial extent of 50 mm, the damage index method results in a large error in Table 5. A different approach shall be followed in order to decompose the superimposed signal so that damage can be quantified in such cases.

4.3. Localisation of corrosion at an arbitrary location in the rebar

In the previous two sections, the damage is maintained at the central location of the rebar. This configuration causes the various scattered waves to arrive at a similar time. Thus, the wave modes are superimposed and result in two distinct wave modes that could be used to develop a damage index. In this section, the location of the pitting corrosion is varied and its effect on the wave characteristics is examined. For this study, an axial extent of 100 mm, and a reduced diameter of 16 mm are chosen for the corrosion. A typical signal in the simulation for the pitting corrosion that is located at a distance 200 mm from the actuator is shown in Fig. 14. Unlike the corrosion that is located equidistant from the actuator and the sensor, the asymmetric corrosion results in multiple wave packets. Typically, four dominant wave packets can be observed due to scattering. These four wave packets are due to reflections from structure boundaries and the damage edges, as shown in Fig. 15. The arrival time of each of these wave packets depends upon the location and the axial extent of the damage. Hence, an estimate of the damage can be made by using these scattered

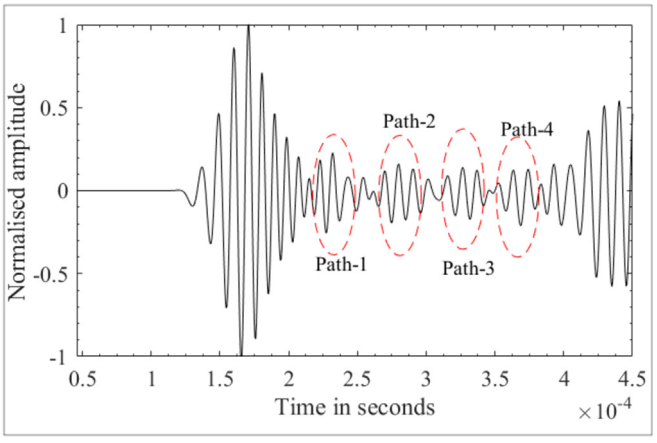

Fig. 14. Response of a rebar with corrosion located at 200 mm from the actuator.

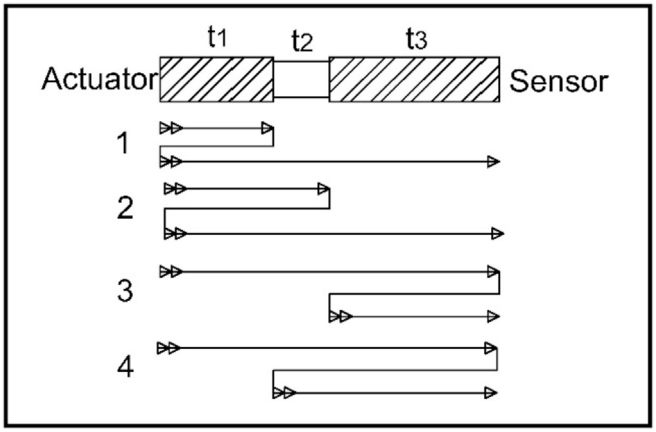

Fig. 15. Schematic diagram displaying the path followed by various scattered wave modes.

waves.

Contrary to the previous cases, in the present case, the arrival time of the scattered waves is not superimposed. Hence, for the damage that is located at an arbitrary location, a different approach is required to estimate the damage. The scattered wave packets that are obtained from the FEA and experimental results for a typical damage that is located at 200 mm from the actuator end are highlighted in Fig. 16. The front edge of the damage can be reconstructed by using the 1st and 4th wave packets, and rear edge can be estimated by using the 2nd and 3rd wave packets. Let T_1, T_2, T_3 and T_4 be the arrival times of each of the wave packets. The location of the front edge of the damage from the actuator end can then be obtained as $x_1 \approx 0.5 \times (L - 0.5 \times (T_4 - T_1) \times V)$, and the location of the rear edge of the damage from the actuator end can be estimated as $x_2 \approx 0.5 \times (L - 0.5 \times (T_3 - T_2) \times V)$. The location and the extent of corrosion that are estimated by this method for various cases are tabulated in Table 6. It is observed that the current method could be applied with considerable accuracy to the detection of damage location. The observed error can be attributed to the difference in the wave velocity in the corroded and intact portions of the rebar, which is not taken into account in the present study. In addition, the possible overlap of the scattered signal with boundary reflections contributes to the shifting of peaks, which results in the error in the length estimation.

4.4. Evaluation of corrosion by using the energy of scattered wave modes

From the previous studies, it is observed that intensity of damage has a direct correlation with the energy of the scattered wave modes. In this section, the factors that affect the scattered energy are studied. A non-dimensional parameter, scatter coefficient (S_{coeff}), is defined as the ratio of the energy of the scattered wave modes of a specimen to the energy of the direct transmitted wave. The total energy of all the wave modes that occur before the arrival of the boundary reflected signal is considered to define this parameter.

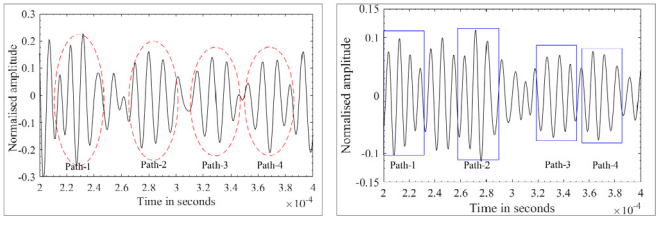

Fig. 16. Scattered wave modes, with paths identified, for a damage located at 200 mm from actuator end from (a) FEA and (b) experiment.

$$S_{coeff} = \sqrt{\int_0^{3T} (S - B)^2 dt / \int_0^{3T} (B)^2 dt} \quad (5)$$

where Time arrival, $T = L/V$

V is the group velocity;
L is the length of the rebar;
S is the signal from the specimen with damage; and
B is the baseline signal.

The scatter coefficient of corroded rebars with a fixed axial extent and intensity is calculated for various locations of damage. The damage that is closer to the sensor results in a higher scatter than that of a damage that is away from the sensor. This observation concurs with the findings that the reflection coefficients diminish with the increase in the distance between the sensor and the damage [34]. Fig. 17 shows the variation of scatter coefficients with the location in the various axial extents of corrosion, with diameter reduction to 16 mm. From this localisation plot, it can be predicted that the increment in the axial extent of corrosion is likely to cause an increase in the scatter coefficient.

In order to define a corrosion damage intuitively, it is essential to quantify it in terms of mass loss. The percentage of mass loss is defined as the weight of material loss due to corrosion in a rebar with respect the initial weight of the rebar. Mass loss in the current case is achieved by reducing the diameter of the rebar for a given axial extent of corrosion. It is observed that scatter coefficient increases with the loss of mass, as shown in Fig. 18, which depicts the variation of the scatter coefficient against the mass loss in a rebar that has a 100 mm-long pitting corrosion.

It is understood that the scatter coefficient is affected by the change in the location, axial extent and intensity of corrosion. Therefore, the axial extents of corrosion can be estimated by using the differential ToF of various scattered wave modes, while the empirical plots for localisation and mass loss, which are presented in this section, can be used to estimate location and intensity of an arbitrary damage.

5. Conclusion

Pitting corrosion of bare reinforcement bars is examined in the current study by using longitudinal guided waves. The response of various corroded bars is studied in order to discern the changes in signal due to corrosion. It is observed that a direct transmitted signal is not affected much by pitting corrosion; hence, it could not be used to identify damage, which, however, can be highlighted by various damage-scattered wave modes. For damage that is located equidistant from the actuator and the sensor, scattered wave modes are superimposed and two distinct wave packets can be observed. A damage index method is thus developed using these two wave packets for assessment.

In order to identify arbitrary pitting corrosion that is located away from the centre, a method is developed by utilising the energy and the time of arrival of scattered wave modes. The arrival time of dominant scattered wave modes is utilised to trace the front and rear edges of the damage. The factors that affect the scattered energy in a corroded rebar are explored by defining a scatter coefficient. It is found that the scatter coefficient gradually increases with the mass loss, and the increment is pronounced when the pitting corrosion is closer to the receiver location. The scatter coefficient when used in conjunction with the localisation method is found to be promising in the assessment of pitting corrosion in reinforcement bars. The current progress in wave propagation mechanism and damage index methods would further help in evaluating the corrosion status of the embedded rebars in concrete. The proposed damage index method would be tested in the future study for the complex geometries of the pitting corrosion and for the rebars embedded in concrete.

Table 6
Location estimation by using the time of arrival of damage edge scattered wave packets.

Sample No.	T1 ($\times 10^{-6}$ s)	T2 ($\times 10^{-6}$ s)	T3 ($\times 10^{-6}$ s)	T4 ($\times 10^{-6}$ s)	×1 (mm)	×2 (mm)	Damage location	Actual Location	Error (%)
FEA results									
1	215.5	262.5	350.0	398.0	108	208	158	150	6%
2	225.0	273.5	329.0	376.0	141	242	192	200	4%
3	253.5	300.5	350.0	389.0	158	248	203	240	15%
Experiment results									
1	212.4	271.7	337.0	371.8	133	231	182	200	9%
2	220.6	264.6	310.0	352.6	161	252	207	250	17%

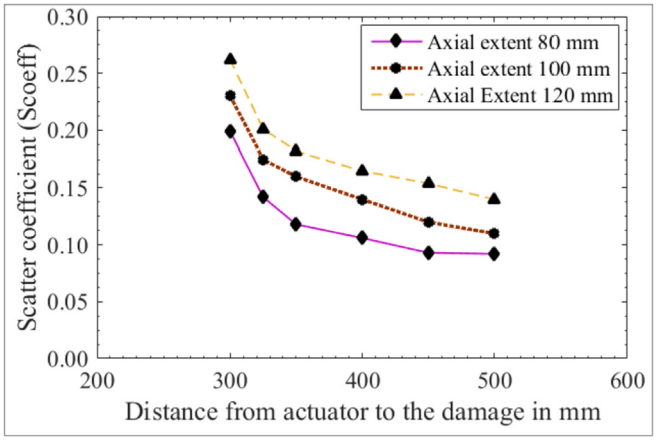

Fig. 17. Localisation plot showing the relationship between the location of the damage and the scatter coefficient.

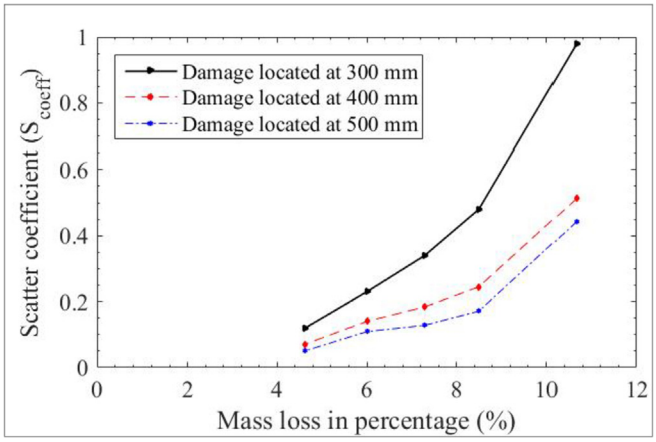

Fig. 18. Mass loss plot showing the relationship between mass loss and scatter coefficient for axial extent 100 mm.

References

[1] Ahmad S. Reinforcement corrosion in concrete structures, its monitoring and service life prediction - a review. Cement Concr Compos 2003;25:459–71. https://doi.org/10.1016/S0958-9465(02)00086-0.

[2] Lu Y, Ye L, Su Z, Huang N. Quantitative evaluation of crack orientation in aluminium plates based on Lamb waves. Smart Mater Struct 2007;16:1907–14. https://doi.org/10.1088/0964-1726/16/5/047.

[3] Wang Y, Guan R, Lu Y. Nonlinear Lamb waves for fatigue damage identification in FRP-reinforced steel plates. Ultrasonics 2017;80:87–95. https://doi.org/10.1016/j.ultras.2017.05.004.

[4] Li J, Lu Y, Guan R, Qu W. Guided waves for debonding identification in CFRP-reinforced concrete beams. Construct Build Mater 2017;131:388–99. https://doi.org/10.1016/j.conbuildmat.2016.11.058.

[5] Sikdar S, Banerjee S, Ashish G. Ultrasonic guided wave propagation and disbond identification in a honeycomb composite sandwich structure using bonded piezoelectric wafer transducers. J Intell Mater Syst Struct 2016;27:1767–79. https://doi.org/10.1177/1045389X15610906.

[6] Rose JL. Ultrasonic guided waves in solid media. Cambridge university press; 2014. https://doi.org/10.1017/CBO9781107273610.

[7] Raghavan A, Cesnik CES. Review of guided-wave structural health monitoring. Shock Vib Digest 2007;39:91–114. https://doi.org/10.1177/0583102406075428.

[8] Rose JL, Ditri JJ, Pilarski A, Rajana K, Carr F. A guided wave inspection technique for nuclear steam generator tubing. NDT E Int 1994;27:307–10. https://doi.org/10.1016/0963-8695(94)90211-9.

[9] Sikdar S, Banerjee S. Identification of disbond and high density core region in a honeycomb composite sandwich structure using ultrasonic guided waves. Compos Struct 2016;152:568–78. https://doi.org/10.1016/j.compstruct.2016.05.064.

[10] Lu Y, Li J, Ye L, Wang D. Guided waves for damage detection in rebar-reinforced concrete beams. Construct Build Mater 2013;47:370–8. https://doi.org/10.1016/j.conbuildmat.2013.05.016.

[11] Mustapha S, Lu Y, Li J, Ye L. Damage detection in rebar-reinforced concrete beams based on time reversal of guided waves. Struct Health Monit 2014;13:347–58. https://doi.org/10.1177/1475921714521268.

[12] Yang Y, Cascante G, Anna Polak M. Depth detection of surface-breaking cracks in concrete plates using fundamental Lamb modes. NDT E Int 2009;42:501–12. https://doi.org/10.1016/j.ndteint.2009.02.009.

[13] Ervin BL, Reis H. Longitudinal guided waves for monitoring corrosion in reinforced mortar. Meas Sci Technol 2008;19:055702https://doi.org/10.1088/0957-0233/19/5/055702.

[14] Sriramadasu RC, Banerjee S, Lu Y. Identification of zero effect state in corroded RCC structures using guided waves and embedded piezoelectric wafer transducers (PWT). Procedia Eng 2017;188:209–16. https://doi.org/10.1016/j.proeng.2017.04.476.

[15] Talakokula V, Bhalla S, Gupta A. Corrosion assessment of reinforced concrete structures based on equivalent structural parameters using electro-mechanical impedance technique. J Intell Mater Syst Struct 2014;25:484–500. https://doi.org/10.1177/1045389X13498317.

[16] Ji YS, Zhao W, Zhou M, Ma HR, Zeng P. Corrosion current distribution of macrocell and microcell of steel bar in concrete exposed to chloride environments. Construct Build Mater 2013;47:104–10. https://doi.org/10.1016/j.conbuildmat.2013.05.003.

[17] Regier R, Hoult NA. Concrete deterioration detection using distributed sensors. Proc Inst Civ Eng - Struct Build 2015;168:118–26. https://doi.org/10.1680/stbu.13.00070.

[18] Amjad U, Yadav SK, Kundu T. Detection and quantification of diameter reduction due to corrosion in reinforcing steel bars. Struct Health Monit 2015;14:532–43. https://doi.org/10.1177/1475921715578315.

[19] Wang X, Tse PW, Mechefske CK, Hua M. Experimental investigation of reflection in guided wave-based inspection for the characterization of pipeline defects. NDT E Int 2010;43:365–74. https://doi.org/10.1016/j.ndteint.2010.01.002.

[20] Tse PW, Wang X. Characterization of pipeline defect in guided-waves based inspection through matching pursuit with the optimized dictionary. NDT E Int 2013;54:171–82. https://doi.org/10.1016/j.ndteint.2012.10.003.

[21] Carandente R, Lovstad A, Cawley P. The influence of sharp edges in corrosion profiles on the reflection of guided waves. NDT E Int 2012;52:57–68. https://doi.org/10.1016/j.ndteint.2012.08.008.

[22] Demma A, Cawley P, Lowe M, Roosenbrand AG, Pavlakovic B. The reflection of guided waves from notches in pipes: a guide for interpreting corrosion measurements. NDT E Int 2004;37:167–80. https://doi.org/10.1016/j.ndteint.2003.09.004.

[23] Cheraghi Nader, Taheri Farid. A damage index for structural health monitoring based on the empirical mode decomposition. J Mech Mater Struct 2007;2:43–62.

[24] Banerjee S, Ricci F, Monaco E, Mal A. A wave propagation and vibration-based approach for damage identification in structural components. J Sound Vib 2009;322:167–83. https://doi.org/10.1016/j.jsv.2008.11.010.

[25] Gazis DC. Three dimensional investigation of the propagation of waves in hollow circular cylinders. II. Numerical results. J Acoust Soc Am 1959;31:573–8. https://doi.org/10.1121/1.1907754.

[26] Sun Z, Zhang L, Rose JL. Flexural torsional guided wave mechanics and focusing in pipe. J Press Vessel Technol 2005;127:471. https://doi.org/10.1115/1.2065587.

[27] Courant R, Friedrichs K, Lewy H. On the partial difference equations of mathematical physics. IBM J Res Dev 1967;11:215–34. https://doi.org/10.1147/rd.112.0215.

[28] Miller T, Hauser CJ, Kundu T. Nondestructive inspection of corrosion and delamination at the concrete-steel reinforcement interface. Nondestruct Eval 2002;2002:121–8. https://doi.org/10.1115/IMECE2002-33493.

[29] Beard MD. Guided wave inspection of embedded cylindrical structures. Imp Coll Dep Mech Eng 2002. [Doctoral dissertation].

[30] Ervin BL, Bernhard JT, Kuchma DA, Reis H. Estimation of general corrosion damage to steel reinforced mortar using frequency sweeps of guided mechanical waves. Insight - Non-Destructive Test Cond Monit 2006;48:682–92. https://doi.org/10.

1784/insi.2006.48.11.682.
[31] Ervin BL, Kuchma DA, Bernhard JT, Reis H. Monitoring corrosion of rebar embedded in mortar using high-frequency guided ultrasonic waves. J Eng Mech 2009;135:9–19. https://doi.org/10.1061/(ASCE)0733-9399(2009)135:1(9).
[32] Pavlakovic B, Lowe MJS. Disperse software. 2005.
[33] Feldman M. Hilbert transform in vibration analysis. Mech Syst Signal Process 2011;25:735–802. https://doi.org/10.1016/j.ymssp.2010.07.018.
[34] Diligent O, Grahn T, Boström A, Cawley P, Lowe MJS. The low-frequency reflection and scattering of the S0 Lamb mode from a circular through-thickness hole in a plate: finite Element, analytical and experimental studies. J Acoust Soc Am 2002;112:2589–601. https://doi.org/10.1121/1.1512292.